PHYSICAL SCIENCES

The primary gas phase hydration shell of hydroxide

Wenjin Cao[1], Hui Wen[1,2], Sotiris S. Xantheas[3,4]*, Xue-Bin Wang[1]*

The number of water molecules in hydroxide's primary hydration shell has been long debated to be three from the interpretation of experimental data and four from theoretical studies. Here, we provide direct evidence for the presence of a fourth water molecule in hydroxide's primary hydration shell from a combined study based on high-resolution cryogenic experimental photoelectron spectroscopy and high-level quantum chemical computations. Well-defined spectra of $OH^-(H_2O)_n$ clusters (n = 2 to 5) yield accurate electron binding energies, which are, in turn, used as key signatures of the underlying molecular conformations. Although the smaller $OH^-(H_2O)_3$ and $OH^-(H_2O)_4$ clusters adopt close-lying conformations with similar electron binding energies that are hard to distinguish, the $OH^-(H_2O)_5$ cluster clearly has a predominant conformation with a four-coordinated hydroxide binding motif, a finding that unambiguously determines the gas phase coordination number of hydroxide to be four.

INTRODUCTION

As one of the fundamental ions in aqueous solutions that governs acid-base chemistry, the hydroxide ion (OH^-) has drawn considerable research interest. For instance, extensive efforts have been reported in past decades to explore its speciation as a function of pH (*1*, *2*), its solvation dynamics (*3*–*6*), and its role in chemical reactions (*7*, *8*). A crucial key to understanding its unique behavior in aqueous ionic solutions is the structure of its solvation shell, which is the number of water molecules in its immediate vicinity (*9*), whose fluctuation leads to the proton transfer that relates to its diffusion. In liquid water, the analysis of neutron diffraction data has suggested the existence of four water molecules in the immediate vicinity of OH^-, with a fifth one weakly bound to its hydroxyl hydrogen (*10*); note, however, that this result was obtained within an empirical potential structure refinement framework. Molecular dynamics simulations predicted a stable fourfold-coordinated motif in the bulk environment, while the first solvation shell H-bond breaking that transforms the four-coordinated hydroxide to transient three-coordinated motif is believed to be the key step to initiate hydroxide diffusion (*3*). To connect molecular level information to macroscopic behavior, the experimental determination of the number of H_2O molecules in hydroxide's primary solvation shell in the gas phase is desired. This is achieved by the successful identification of conformations of size-selected microsolvated $OH^-(H_2O)_n$ clusters.

As an effective tool to address such a challenge, gas phase ion spectroscopic techniques have been previously used to investigate such clusters decades ago (*11*). A breakthrough occurred in 2003, when Johnson and coworkers (*12*–*14*) carried out a series of Ar or H_2-tagged infrared (IR) predissociation studies on hydrated OH^- clusters with up to five H_2O molecules attached. These studies provided experimental evidence for the number of H_2O molecules in the primary solvation shell of OH^- by identifying signature vibrational modes of inter-water hydrogen bonds in the 3-μm IR OH region, whose existence indicated that additional water molecules were attached outside the primary solvation shell instead of directly to the OH^- core (*12*). During these studies, the number of water molecules in hydroxide's primary solvation shell was determined to be three, since inter-water hydrogen bonds appeared upon the addition of the fourth water molecule (*12*). This is in contrast to the findings of subsequent high-level quantum chemical calculations, which predicted a four-coordinated OH^- (*15*, *16*). However, because of the close-lying energies of the three- and four-coordinated complexes for $OH^-(H_2O)_4$ (*15*), both types of isomers were predicted to coexist even under cryogenic conditions. The measured vibrational spectra confirmed the existence of the three-coordinated isomer, while the possibility to coexist with the four-coordinated isomer could not be completely discarded. For larger clusters, such as $OH^-(H_2O)_5$, inter-water hydrogen bond would always be present for either three- or four-coordinated isomers, making it even more difficult to determine the number of water molecules in the primary solvation shell in these complexes. To date, the structures of $OH^-(H_2O)_n$ clusters are far less understood compared to those of the proton (*17*–*19*). Definitive spectroscopic studies, especially on larger clusters, are still warranted to resolve this controversy.

Photoelectron spectroscopy is also a powerful tool that can be used to probe the structural and energetic properties of microsolvated clusters (*20*). Unexpectedly, after almost two decades from the previous IR study, no photoelectron spectrum has been reported for $OH^-(H_2O)_n$ clusters, except for the binary $OH^-(H_2O)$ complex (*21*–*23*). Current advances in cryogenic techniques have resulted in improved spectral resolution (*23*), further establishing the importance of the method as a benchmark for high-level quantum dynamics simulations, such as the ones reported for $OH^-(H_2O)$ (*24*, *25*). Although less sensitive in probing molecular vibrations, photoelectron spectroscopy is also capable of yielding the electron binding energies (EBEs). In addition, the possible existence of inter-water hydrogen bonds in larger $OH^-(H_2O)_n$ clusters has limited their structural assignment via traditional IR methods, whereas the variations in binding strengths that determine the stability of a certain isomer could lead to distinct EBEs. Therefore,

[1]Physical Sciences Division, Pacific Northwest National Laboratory, Richland, WA 99352, USA. [2]Laboratory of Atmospheric Physico-Chemistry, Hefei Institutes of Physical Science, Chinese Academy of Sciences, Hefei, Anhui 230031, China. [3]Advanced Computing, Mathematics and Data Division, Pacific Northwest National Laboratory, Richland, WA 99352, USA. [4]Department of Chemistry, University of Washington, Seattle, WA 98195, USA.
*Corresponding author. Email: xuebin.wang@pnnl.gov (X.-B.W.); sotiris.xantheas@pnnl.gov (S.S.X.)

the structural characterization of cluster isomers from photoelectron spectra could be the key to a better understanding of the $OH^-(H_2O)_n$ conformers. For larger $OH^-(H_2O)_n$ clusters, the photoelectron spectra have only been theoretically simulated (*26*, *27*), while the accuracy in these calculations and simulations still needs to be validated by experimental measurements.

Here, we present a joint study based on cryogenic negative ion photoelectron spectroscopy (NIPES) (*28*) and high-level quantum chemical computations for the microsolvated $OH^-(H_2O)_n$ clusters (n = 2 to 5) and provide direct evidence for the presence of four water molecules in hydroxide's primary solvation shell. In this work, NIPE spectra of these clusters were obtained, yielding vertical detachment energies (VDEs) and upper limits of adiabatic detachment energies (ADEs) and their stepwise increments upon sequential addition of water molecules. The NIPE spectra were assigned to conformers with the aid of high-level ab initio quantum chemical calculations at the second-order Møller-Plesset perturbation (MP2) (*29*) and the coupled cluster including single, double, and perturbative triple excitations [CCSD(T)] (*30*, *31*) levels of theory using Dunning's augmented correlation-consistent aug-cc-pVnZ (hereafter denoted as aVnZ, n = D − Q) basis sets (*32*). The $OH^-(H_2O)_3$ and $OH^-(H_2O)_4$ were found to have multiple isomers with different structural motifs associated with close-lying relative energies and VDEs and can therefore coexist. For $OH^-(H_2O)_5$, the isomer with hydroxide adopting a fourfold coordination has been unambiguously assigned, revealing a number of four water molecules in hydroxide's primary gas phase solvation shell.

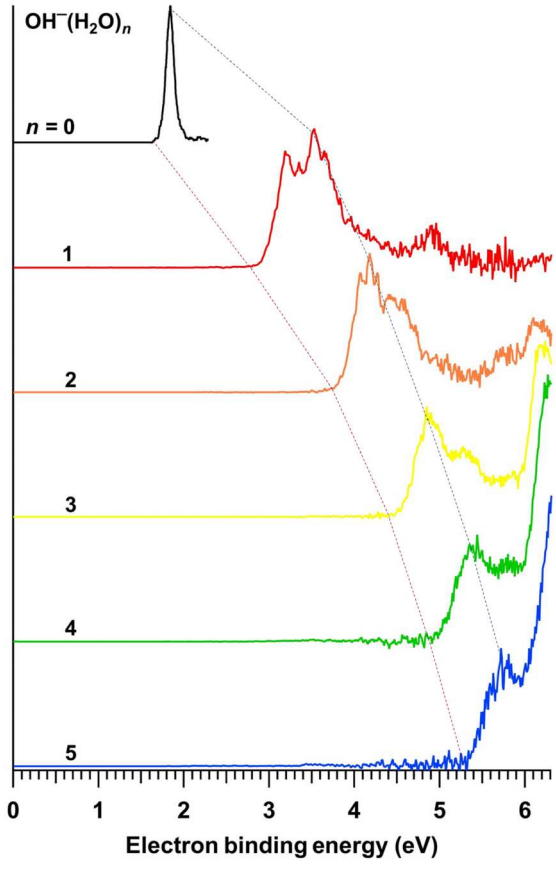

Fig. 1. NIPE spectra of isolated OH^- and $OH^-(H_2O)_n$ clusters (n = 1 to 5). The spectra of isolated OH^- (black trace) and $OH^-(H_2O)$ (red trace) were adapted from (*33*, *23*), respectively, while those of $OH^-(H_2O)_n$ (n = 2 to 5) were measured at T = 20 K with a 193-nm (6.424 eV) incident photon energy. The dotted lines trace the trends in the stepwise ADE (brown) and VDE (navy) energy shifts with cluster size.

RESULTS AND DISCUSSION

NIPE spectra of $OH^-(H_2O)_n$ (n = 2 to 6)

Figure 1 shows the T = 20 K NIPE spectra of solvated hydroxide clusters with up to five water molecules. The spectra of isolated OH^- (*33*) and the binary $OH^-(H_2O)$ cluster (*23*) adopted from previous studies are also included for comparison. The isolated OH^- has a relatively simple spectrum with a VDE of 1.88 eV (*33*), while its ADE is more precisely measured at 1.83 eV (Table 1) (*34*–*36*). With one water molecule attached, the $OH^-(H_2O)$ cluster has a spectrum with at least two vibrational progressions that are assigned to the proton asymmetric stretching mode and its coupling with the proton bending and the O—O symmetric stretching modes, respectively, identified by combining the NIPES measurements with a four-dimensional Franck-Condon simulation (*23*). This assignment is further supported by a full-dimensional quantum chemical study (*25*).

The $OH^-(H_2O)_2$ spectrum is slightly more complex, with both the ADE and VDE further blue-shifted to 3.85 and 4.18 eV, respectively. It is worth noting that the ADE measured here corresponds to the upper limit of the true ADE, since the 0-0 transition from the anionic to the neutral vibrational ground state that represents the true ADE may have negligible intensity due to the large anion-to-neutral geometry change. The spectrum shows a major progression with the interval of ~0.3 eV (2420 cm^{-1}) and the first band further splitting into three peaks at 4.07, 4.18, and 4.27 eV, respectively, while the higher EBE band is barely resolved. The ADEs (upper limits)/VDEs of the $OH^-(H_2O)_3$ and $OH^-(H_2O)_4$ clusters are measured to be 4.50/4.85 and 4.95/5.36 eV, respectively. Their NIPE spectra are even more complex, each resolving only two broad features and some signal near the photodetachment energy limit. The spectrum of $OH^-(H_2O)_3$ shows a band centered at 5.32 eV next to the 4.85-eV strongest band, while the one for the $OH^-(H_2O)_4$ cluster exhibits an additional band centered around 5.8 eV in addition to the vertical transition at 5.36 eV. The spectrum of $OH^-(H_2O)_5$ is largely truncated because of the photodetachment energy limit and exhibits a VDE of 5.72 eV and an ADE upper limit of 5.30 eV. For the larger $OH^-(H_2O)_n$ clusters, the EBEs shift to an even higher energy range lying outside the photodetachment energy limit, thus preventing the recording of their photoelectron spectroscopy spectra to obtain the experimental VDEs. Nevertheless, a rough spectrum collected for $OH^-(H_2O)_6$ shows a rising edge at 5.65 eV (see fig. S1).

Upon sequential hydration, the blue shifts in the ADE (upper limit)/VDE values of $OH^-(H_2O)_n$ clusters are recorded (Table 1). With one water molecule attached, the Δ(ADE)/Δ(VDE) values are as large as 1.07/1.65 eV. For n = 2, a sizeable Δ(ADE) of 0.95 eV is recorded, while the Δ(VDE) is relatively smaller (0.65 eV). For the larger clusters, both the Δ(ADE)s and Δ(VDE)s gradually decrease and become similar to each other, i.e., 0.65/0.67, 0.45/0.51, and 0.35/0.36 eV for the Δ(ADE)/Δ(VDE) for the n = 3, 4, and 5 clusters, respectively. For $OH^-(H_2O)_6$, a Δ(ADE) of 0.35 eV has been recorded. These stepwise shifts in the EBEs, especially

Table 1. Experimental (expt.) and calculated (calc.) ADE /VDE values (in eV) of the $OH^-(H_2O)_n$ (n = 1 to 6) clusters. The calculations were carried out at the CCSD(T)//MP2 level of theory with the aug-cc-pVTZ basis set. The values in parentheses correspond to the Δ(ADE)/Δ(VDE) values obtained from the ADE/VDE differences relative to the $OH^-(H_2O)_{n-1}$ cluster.

n	ADE		VDE	
	Expt.	Calc.	Expt.	Calc.
0	1.83*	–	1.88†	–
1	2.90 ± 0.05‡ (1.07)	2.79	3.53 ± 0.02‡ (1.65)	3.59
2	3.85 ± 0.05 (0.95)	3.26	4.18 ± 0.02 (0.65)	4.35 (0.76)
3	4.50 ± 0.05 (0.65)	–	4.85 ± 0.05 (0.67)	4.94 (0.59§)
4	4.95 ± 0.05 (0.45)	–	5.36 ± 0.05 (0.51)	5.58 (0.64§)
5	5.30 ± 0.05 (0.35)	–	5.72 ± 0.05 (0.36)	5.96 (0.38§)
6	5.65 ± 0.05 (0.35)	–	–	–

*Reference (*36*). †Reference (*33*). ‡Reference (*23*). §The calculated Δ(VDE) is only reported for the most stable isomer of each complex; see Figs. 2 and 4 for the VDE/Δ(VDE)s of less stable isomers.

ADE, serve as important indicators for the sequential binding energies of the cluster. The trend in Δ(ADE) reported herein qualitatively correlates with the sequential binding energies, measured in a previous kinetics study as 1.15, 0.76, 0.70, 0.52, 0.50, and 0.49 eV for n = 1 to 6 $OH^-(H_2O)_n$ clusters, respectively (*37*).

Benchmark calculations

The geometries of the $OH^-(H_2O)_n$ clusters have been previously extensively studied theoretically using quantum chemical calculations at various levels of theory (*15*, *16*, *26*, *27*, *38*). As a result of these studies, a general consensus was reached that for smaller clusters, because of the negative charge on the hydroxyl oxygen, which makes it an ideal hydrogen bond acceptor, all water molecules directly bind to the OH^- core until filling up the primary hydration shell. To predict the number of water molecules in the primary solvation shell, Xantheas and coworkers (*15*, *38*) have reported ab initio calculations of the $OH^-(H_2O)_n$ clusters (n = 1 to 5) with different hydroxide coordination numbers. The optimized geometries reported in these studies were selected as initial guess for refinement in the current study. In $OH^-(H_2O)_2$, the two water molecules bind symmetrically to the hydroxide, each of which forming one O—H···O hydrogen bond between the hydrogen of the water molecule and the oxygen of the hydroxide (Fig. 2). Each of the water molecules is strongly bound to OH^- as attested by the nearly linear hydrogen bond (O—H—O angle of 177.2°), which is similar to the one in the $OH^-(H_2O)$ cluster. However, the O—H bond in the water molecule that interacts with OH^- is less distorted, and this proton remains closer to the oxygen atom of water instead of being shared by the two adjacent O atoms as in the case of $OH^-(H_2O)$. This is indicative of a weaker hydrogen bond compared to that in $OH^-(H_2O)$. Such a prediction parallels with the smaller Δ(ADE)/Δ(VDE) of 0.95/0.65 eV for $OH^-(H_2O)_2$ compared to 1.07/1.65 eV for $OH^-(H_2O)$. On the other hand, upon the removal of the excess negative charge on the hydroxyl group, the neutral $OH(H_2O)_2$ complex adopts a ring structure formed by hydroxyl radical and the two water molecules (fig. S2).

On the basis of our previous investigation of the $OH^-(H_2O)$ complex, an effective "convergence" (<0.05 eV) of the VDE/ADE has been achieved from the CCSD(T)//MP2 calculations with the aug-cc-pVTZ(aVTZ) basis set. A similar conclusion has been drawn for the calculated VDE values of $OH^-(H_2O)_2$, as shown in Fig. 3. MP2 overestimates the VDE by at least 0.3 eV, whereas a better agreement with experiment is obtained for the CCSD(T) and CCSD(T)//MP2 [CCSD(T) energy at the MP2 optimized geometry] calculations. Notably, the results with the aVTZ and aug-cc-pVQZ(aVQZ) basis sets are within <0.05 eV of each other, reinforcing the achievement of effective convergence with the aVTZ basis set. The computed VDEs of 4.35 and 4.26 eV based on CCSD(T)//MP2 and CCSD(T) calculations with the aVTZ basis set are both in reasonable agreement with the experimental value of 4.18 eV. However, in terms of ADEs, none of the methods used here provides a good agreement with the experimental value of 3.85 eV, as both the CCSD(T) and CCSD(T)//MP2 results underestimate the ADE by at least 0.5 eV. Since the experimental estimate only corresponds to the upper limit of the true ADE, it is likely that the geometry change, shown in fig. S2, is substantial enough to completely hinder the intensity of the 0-0 transition, thus preventing the quantitative comparison between the experimental and computed ADEs. Because of this limitation, only the VDEs are computed and compared with the experimental values for the larger $OH^-(H_2O)_n$ clusters. The benchmark study for $OH^-(H_2O)_2$ reported here, combined with the previous one for $OH^-(H_2O)$ (*23*) and additional benchmarks for CCSD(T) optimized versus CCSD(T)//MP2 energies for $OH^-(H_2O)_3$ (see tables S1 and S2),

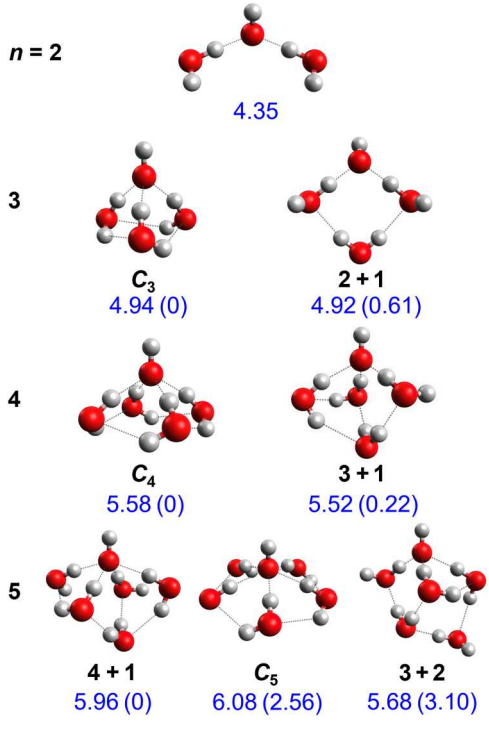

Fig. 2. Optimized low-lying isomers of the $OH^-(H_2O)_n$ (n = 2 to 5) cluster anions. Optimized geometries at the MP2/aug-cc-pVTZ level of theory, along with their CCSD(T)//MP2 VDEs (in eV) and relative energies (kcal/mol) in parentheses, both labeled in blue. Dotted lines indicate the hydrogen bonds.

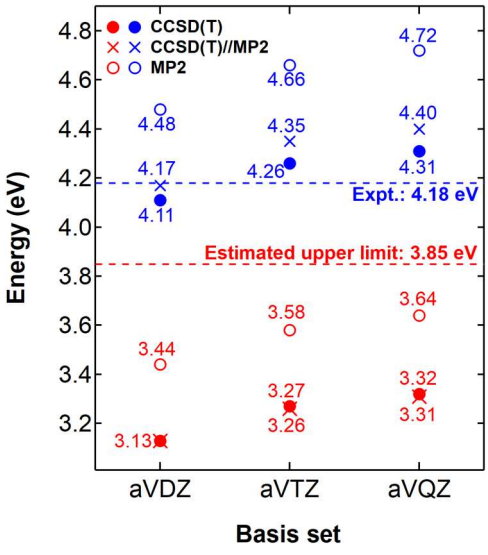

Fig. 3. The benchmark on $OH^-(H_2O)_2$ VDE and ADE. Calculated ADEs (red) and VDEs (blue) at the MP2 (open circles), CCSD(T) (filled circles), and CCSD(T)//MP2 (crosses) levels of theory for the $OH^-(H_2O)_2$ anion with the correlation consistent basis sets of double through quadruple zeta quality. The experimentally estimated upper limits of the ADE and measured VDE are denoted with red and blue dashed lines, respectively.

demonstrates that CCSD(T)//MP2 with the aVTZ basis set represents an accurate and cost-efficient protocol in evaluating both relative energies of different isomers (for example, within an accuracy of <0.1 kcal/mol for the $n = 3$ cluster) and VDEs and is therefore used for the larger clusters.

Determination of hydroxide primary hydration shell

For the larger $OH^-(H_2O)_n$ clusters, different structural motifs corresponding with various conformations exist, such as those with all water molecules bound directly to hydroxide within the primary solvation shell or with a certain number of water molecules in the primary solvation shell and others in the secondary solvation shell. The former isomers for the $OH^-(H_2O)_n$ ($n = 3$ to 5) clusters are highly symmetric (labeled $\boldsymbol{C_n}$, as they exhibit structures with highly symmetric point groups). On the other hand, the latter isomers are labeled as "$x + y$," where x and y denote the number of water molecules within and outside the primary solvation shell, respectively.

For the $OH^-(H_2O)_3$ cluster, the most stable isomer is $\boldsymbol{C_3}$, in which all three water molecules are bound directly to OH^-. The other isomer, **2 + 1**, with two of the water molecules directly hydrogen bonded to hydroxide and the third one hydrogen bonded to the O atoms of the other two, is slightly higher in energy by 0.61 kcal/mol. Moreover, the two different types of isomers have near identical calculated VDEs of 4.94 eV ($\boldsymbol{C_3}$) and 4.92 eV (**2 + 1**), both of which are in good agreement with the measured value of 4.85 eV. Since it has been demonstrated that less thermodynamically stable species generated at room temperature could be kinetically isolated and detected under low temperature in our ion source (*39*), both isomers could coexist and can be attributed to the measured spectrum. The situation is similar when one additional water molecule is present: The two low-lying isomers, $\boldsymbol{C_4}$ and **3 + 1**, of the $OH^-(H_2O)_4$ cluster are also nearly isoenergetic based on CCSD(T)//MP2 estimates. The $\boldsymbol{C_4}$ isomer, with all four water molecules directly hydrogen bonded to the hydroxide, is predicted to be more stable by 0.22 kcal/mol than the **3 + 1** isomer, which has a three-coordinated hydroxide binding motif and a water molecule in the second solvation shell. Such a small energy difference supports the possibility for the coexistence of these two isomers, since they could both be kinetically trapped and detected during the experiment. The corresponding calculated VDEs of 5.58 eV ($\boldsymbol{C_4}$) and 5.52 eV (**3 + 1**) are also quite close to each other and are both within ~0.2 eV from the experimental value of 5.36 eV (Fig. 4). This suggests that both isomers could be possibly attributed to the experimental spectrum, as they cannot be distinguished due to the close-lying relative energies and VDEs. Johnson and coworkers (*12*) have previously confirmed the presence of the **3 + 1** isomer from the observation of vibrational signatures that are associated with inter-water hydrogen bonds. However, the possibility of coexistence between the $\boldsymbol{C_4}$ and **3 + 1** isomers remains unclear and unsettled. Moreover, with more water molecules added, it becomes even more challenging to determine the number of molecules in the first solvation shell based on the vibrational signatures of inter-water hydrogen bonds, as the water hydrogen bond network becomes common for larger clusters regardless of the coordination number of the hydroxide. With more water molecules added, a clear energy gap between different types of isomers for a certain complex is expected, when the primary solvation shell is filled up, a matter that still remains to be explored.

Such an energy gap is seen for $OH^-(H_2O)_5$. Various isomers with the hydroxide adopting coordination numbers of 3, 4, and 5, labeled as **3 + 2**, **4 + 1**, and $\boldsymbol{C_5}$, respectively, have been found (Fig. 2). On the basis of the CCSD(T)//MP2 calculations, **4 + 1** is the most favored isomer with an energy advantage of at least 2.56 kcal/mol

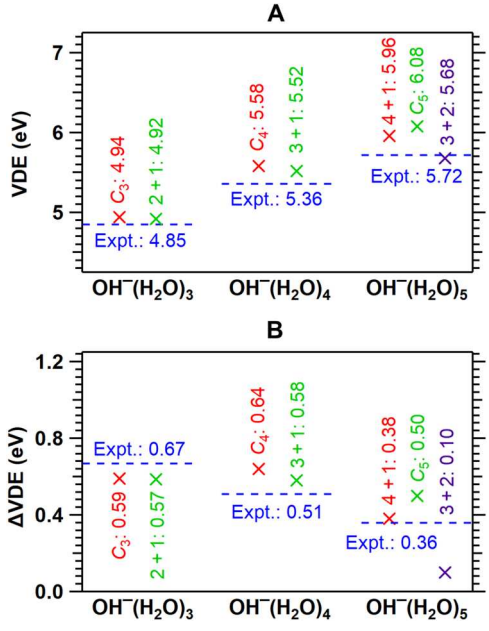

Fig. 4. VDEs of the various conformations for the $OH^-(H_2O)_n$ ($n = 2$ to 5) clusters. Comparison between the experimental (blue dashed lines) and calculated CCSD(T)//MP2 (colored crosses) values of (**A**) VDE and (**B**) Δ(VDE) of the $OH^-(H_2O)_n$ clusters ($n = 3$ to 5). The displayed calculated Δ(VDE) of each isomer is based on the VDE difference compared to the most stable n-1 isomer.

compared to either C_5 or **3 + 2** isomers, a result that strongly indicates the dominance of the four-coordinated **4 + 1** isomer over the other two. This is further confirmed by comparing the computed and measured VDEs. Different from $OH^-(H_2O)_3$ and $OH^-(H_2O)_4$, the three isomers of $OH^-(H_2O)_5$ have distinct calculated VDE values, with the C_5 isomer having the largest computed VDE of 6.08 eV, followed by **4 + 1** at 5.96 eV and **3 + 2** at 5.68 eV (Fig. 4A). The C_5 isomer could be first excluded due to its higher energy relative to **4 + 1** and the overestimation of the VDE compared to the experimental value at 5.72 eV. Isomer **3 + 2**, which is also higher in energy relative to **4 + 1**, while with a seemingly good agreement between the theoretical and experimental VDEs, exhibits substantial discrepancy in the Δ(VDE). Compared to the theoretical VDEs of $OH^-(H_2O)_4$, which are 5.58 eV for C_4 and 5.52 eV for **3 + 1**, the calculated Δ(VDE) of this isomer is in the range of 0.10 to 0.16 eV, far below the measured value of 0.36 eV (Fig. 4B). The most stable isomer **4 + 1**, on the other hand, exhibits good agreement with the experimentally measured values for both calculated VDE and Δ(VDE) (Fig. 4). Therefore, the experimental spectrum could be unambiguously assigned to the contribution solely from **4 + 1**. The preference of four-coordinated isomer against three- or five-coordinated ones in the $OH^-(H_2O)_5$ complex serves as a direct evidence in the existence of a fourth water molecule in hydroxide's first solvation shell. Notably, both the **3 + 1** and C_4 isomers coexist in our experiment, an observation that is consistent with the previous IR-tagging study (*12*). However, our CCSD(T)//MP2 calculations indicate the C_4 isomer being slightly more stable, a conclusion that is further supported by the dominant **4 + 1** structure in the $n = 5$ cluster.

To conclude, a joint photoelectron spectroscopy and quantum chemical study of microsolvated hydroxide ion clusters with up to five water molecules provides direct evidence for a four-coordinated gas phase hydroxide primary solvation shell. This was achieved by the assignment of the NIPE spectral profiles for the $OH^-(H_2O)_n$ ($n = 2$ to 5) clusters and the subsequent assignment of structural motifs based on the comparison between the calculated and the experimentally measured VDEs and their stepwise increments. In addition, the upper limit of ADE of each cluster is also estimated. High-level electronic structure computations of the VDEs/ADEs for the $n = 1$ and 2 clusters at the CCSD(T)//MP2 level with the aVTZ basis set have identified this protocol as an accurate and computationally efficient approach to reproduce the measured data. This level of theory was subsequently used to probe isomers with different coordination motifs for the larger clusters. The partially vibrationally resolved spectra of $OH^-(H_2O)_2$ and $OH^-(H_2O)_3$ provide crucial spectroscopic signatures to benchmark their complex multidimensional potential energy surfaces in both the anionic and neutral states. On the basis of the comparisons between the experimental spectra and the calculated relative isomer energies and VDEs, the coexistence of two structural motifs for $OH^-(H_2O)_3$ and $OH^-(H_2O)_4$ is possible. In contrast, for $OH^-(H_2O)_5$, the isomer with the hydroxide ion in a fourfold coordination is found to dominate over the three- or five-coordinated ones due to the favorable thermal energies and the distinct VDEs, thus providing solid evidence for the presence of four water molecules in hydroxide's first solvation shell. This finding is in accordance with the structural motifs previously suggested from experimental neutron diffraction data (*10*) and molecular simulations of aqueous hydroxide solutions (*3*, *9*), suggesting a similarity of the water coordination structure around hydroxide in the cluster and solution phase environments. This work further establishes the synergism between NIPES and high-level electronic structure theory as an effective tool toward providing a better understanding of the microsolvation mechanism of hydroxide at the molecular level. It also shows that the local hydration motif of hydroxide in an aqueous solution is qualitatively similar to the one found in a cluster environment, a finding that further underpins the importance of molecular clusters in providing molecular level structural motifs found in condensed environments.

MATERIALS AND METHODS

Negative ion photoelectron spectroscopy

NIPE spectra were obtained using a magnetic bottle time-of-flight (TOF) photoelectron spectrometer combined with an electrospray ionization (ESI) source and a temperature-controlled cryogenic ion trap, as described elsewhere (*28*). The $OH^-(H_2O)_n$ cluster anions were generated by electrospraying ~0.1 mM acetonitrile/water (3:1, v/v) NaOH solutions. The resulting anions were transported by a radio frequency quadrupole ion guide and first detected by a quadrupole mass spectrometer, during which the ESI conditions were optimized to ensure stable and intense ion cluster beams. A 90° bender was used to direct the anions into the cryogenic three-dimensional ion trap where they were accumulated for 20 to 100 ms and cooled by collisions with a cold buffer gas (20% H_2 balanced in He) to 20 K, before being pulsed-out into the extraction zone of the TOF mass spectrometer for mass analysis at a repetition rate of 10 Hz. The $OH^-(H_2O)_n$ cluster anions were mass-selected and decelerated before being photodetached by a probe laser beam in the interaction zone of the magnetic bottle photoelectron analyzer. A 193-nm (6.424 eV, Lambda Physics Complex 100 ArF) laser beam, operated at a 20-Hz repetition rate with the anion beam shut off on alternating laser shots to afford shot-to-shot background subtraction, was used for photodetachment. The resulting photoelectrons were collected at nearly 100% efficiency in the magnetic bottle and analyzed with a 5.2-m-long electron flight tube. Recorded flight times were converted into calibrated kinetic energies using the known spectra of $I^-/OsCl_6^{2-}$ (*40*, *41*). EBEs were obtained by subtracting the electron kinetic energies from the detachment photon energy with an electron energy resolution ($\Delta E/E$) of about 2% (i.e., ~20 meV for 1 eV kinetic energy electrons).

Computational details

For the smallest $OH^-(H_2O)_2$ anion in this family of clusters, its geometric structures of both anionic and neutral states were optimized at the MP2 (*29*) and CCSD(T) (*30*, *31*) levels of theory using the family of Dunning's augmented correlation-consistent aV*n*Z (n = D and T) basis sets (*32*). To further refine the computed electronic energies, single-point energy calculations for both the anion and the neutral radical were carried out with the aVQZ basis set at the corresponding aVTZ-optimized geometries. Single-point CCSD(T) calculations were also performed at the MP2-optimized geometries [CCSD(T)//MP2] for each basis (except for the aVQZ, which used MP2/aVTZ-optimized geometries) as a comparison to assess the accuracy of MP2-optimized structures with respect to those optimized with CCSD(T). The use of the CCSD(T)//MP2 protocol has been previously shown to be an accurate and efficient approach for hydrogen-bonded systems (*42*, *43*). Additional CCSD(T)/aVTZ geometry optimization was performed for

$OH^-(H_2O)_3$. Theoretical ADEs or VDEs were obtained at each theory/basis set level by calculating energy differences between the neutral and anionic energies at the respective optimized geometries including harmonic zero-point energy (ZPE) corrections or at the optimized anionic geometries. While for larger $OH^-(H_2O)_n$ clusters (n = 3 to 5), only anionic geometries were optimized at the MP2/aVTZ level of theory due to the considerations of computational costs and the benchmark studies on $OH^-(H_2O)$ (*23*) and $OH^-(H_2O)_2$ that demonstrated sufficient accuracy in geometric structures. Nevertheless, CCSD(T)/aVTZ single-point calculations were still carried out for both anionic and neutral complexes at the MP2/aVTZ-optimized anionic geometries to provide CCSD(T)//MP2 VDEs. Initial guesses for the input geometries were made on the basis of optimized structures from previous works (*15*, *38*). For each cluster, multiple types of conformations with various hydroxide coordination numbers were considered. The relative energies of different isomers were compared on the basis of the energies obtained from the CCSD(T)//MP2 calculations coupled with the aVTZ basis set, including the harmonic MP2 ZPE corrections. All calculations were performed using the NWChem software package (*44*). The CCSD(T) calculations for the open shell neutral were performed with the Tensor Contraction Engine module in NWChem (*45*–*49*).

Supplementary Materials

This PDF file includes:

Tables S1 and S2

Figs. S1 and S2

REFERENCES AND NOTES

1. D. Strmcnik, M. Uchimura, C. Wang, R. Subbaraman, N. Danilovic, D. van der Vliet, A. P. Paulikas, V. R. Stamenkovic, N. M. Markovic, Improving the hydrogen oxidation reaction rate by promotion of hydroxyl adsorption. *Nat. Chem.* **5**, 300–306 (2013).
2. K. C. Ng, T. Adel, K. U. Lao, M. G. Varmecky, Z. Liu, M. Arrad, H. C. Allen, Iron(III) chloro complexation at the air–aqueous $FeCl_3$ interface via second harmonic generation spectroscopy. *J. Phys. Chem. C* **126**, 15386–15396 (2022).
3. M. E. Tuckerman, D. Marx, M. Parrinello, The nature and transport mechanism of hydrated hydroxide ions in aqueous solution. *Nature* **417**, 925–929 (2002).
4. E. F. Aziz, N. Ottosson, M. Faubel, I. V. Hertel, B. Winter, Interaction between liquid water and hydroxide revealed by core-hole de-excitation. *Nature* **455**, 89–91 (2008).
5. C. Chen, Y.-L. S. Tse, G. E. Lindberg, C. Knight, G. A. Voth, Hydroxide solvation and transport in anion exchange membranes. *J. Am. Chem. Soc.* **138**, 991–1000 (2016).
6. M. Chen, L. Zheng, B. Santra, H.-Y. Ko, R. A. DiStasio Jr., M. L. Klein, R. Car, X. Wu, Hydroxide diffuses slower than hydronium in water because its solvated structure inhibits correlated proton transfer. *Nat. Chem.* **10**, 413–419 (2018).
7. D. T. Sawyer, J. L. Roberts, Hydroxide ion: An effective one-electron reducing agent? *Acc. Chem. Res.* **21**, 469–476 (1988).
8. C.-T. Dinh, T. Burdyny, M. G. Kibria, A. Seifitokaldani, C. M. Gabardo, F. P. García de Arquer, A. Kiani, J. P. Edwards, P. De Luna, O. S. Bushuyev, C. Zou, R. Quintero-Bermudez, Y. Pang, D. Sinton, E. H. Sargent, CO_2 electroreduction to ethylene via hydroxide-mediated copper catalysis at an abrupt interface. *Science* **360**, 783–787 (2018).
9. D. Marx, A. Chandra, M. E. Tuckerman, Aqueous basic solutions: Hydroxide solvation, structural diffusion, and comparison to the hydrated proton. *Chem. Rev.* **110**, 2174–2216 (2010).
10. A. Botti, F. Bruni, S. Imberti, M. A. Ricci, A. K. Soper, Solvation shell of OH^- ions in water. *J. Mol. Liq.* **117**, 81–84 (2005).
11. C. Chaudhuri, Y. S. Wang, J. C. Jiang, Y. T. Lee, H. C. Chang, G. Niedner-Schatteburg, Infrared spectra and isomeric structures of hydroxide ion-water clusters $OH^-(H_2O)_{1\text{-}5}$: A comparison with $H_3O(H_2O)_{1\text{-}5}$. *Mol. Phys.* **99**, 1161–1173 (2001).
12. W. H. Robertson, E. G. Diken, E. A. Price, J.-W. Shin, M. A. Johnson, Spectroscopic determination of the OH^- solvation shell in the $OH^-(H2O)_n$ clusters. *Science* **299**, 1367–1372 (2003).
13. E. G. Diken, J. M. Headrick, J. R. Roscioli, J. C. Bopp, M. A. Johnson, A. B. McCoy, Fundamental excitations of the shared proton in the $H_3O_2^-$ and $H_5O_2^+$ complexes. *J. Phys. Chem. A* **109**, 1487–1490 (2005).
14. O. Gorlova, J. W. DePalma, C. T. Wolke, A. Brathwaite, T. T. Odbadrakh, K. D. Jordan, A. B. McCoy, M. A. Johnson, Characterization of the primary hydration shell of the hydroxide ion with H_2 tagging vibrational spectroscopy of the $OH^-\cdot(H_2O)_{n=2,3}$ and $OD^-\cdot(D_2O)_{n=2,3}$ clusters. *J. Chem. Phys.* **145**, 134304 (2016).
15. X. Sun, S. Yoo, S. S. Xantheas, L. X. Dang, The reorientation mechanism of hydroxide ions in water: A molecular dynamics study. *Chem. Phys. Lett.* **481**, 9–16 (2009).
16. J. J. Novoa, F. Mota, C. Perez del Valle, M. Planas, Structure of the first solvation shell of the hydroxide anion. A model study using $OH^-(H_2O)_n$ (n = 4, 5, 6, 7, 11, 17) clusters. *J. Phys. Chem. A* **101**, 7842–7853 (1997).
17. J.-W. Shin, N. I. Hammer, E. G. Diken, M. A. Johnson, R. S. Walters, T. D. Jaeger, M. A. Duncan, R. A. Christie, K. D. Jordan, Infrared signature of structures associated with the $H^+(H_2O)_n$ (n = 6 to 27) clusters. *Science* **304**, 1137–1140 (2004).
18. J. M. Headrick, E. G. Diken, R. S. Walters, N. I. Hammer, R. A. Christie, J. Cui, E. M. Myshakin, M. A. Duncan, M. A. Johnson, K. D. Jordan, Spectral signatures of hydrated proton vibrations in water clusters. *Science* **308**, 1765–1769 (2005).
19. H. J. Zeng, M. A. Johnson, Demystifying the diffuse vibrational spectrum of aqueous protons through cold cluster spectroscopy. *Annu. Rev. Phys. Chem.* **72**, 667–691 (2021).
20. X.-B. Wang, Cluster model studies of anion and molecular specificities via electrospray ionization photoelectron spectroscopy. *J. Phys. Chem. A* **121**, 1389–1401 (2017).
21. D. W. Arnold, C. Xu, D. M. Neumark, Spectroscopy of the transition state: Elementary reactions of the hydroxyl radical studied by photoelectron spectroscopy of $O^-(H_2O)$ and $H_3O_2^-$. *J. Chem. Phys.* **102**, 6088–6099 (1995).
22. H.-J. Deyerl, A. Khai Luong, T. G. Clements, R. E. Continetti, Transition state dynamics of the OH + H_2O hydrogen exchange reaction studied by dissociative photodetachment of $H_3O_2^-$. *Faraday Discuss.* **115**, 147–160 (2000).
23. W. Cao, S. S. Xantheas, X.-B. Wang, Cryogenic vibrationally resolved photoelectron spectroscopy of $OH^-(H_2O)$: Confirmation of multidimensional Franck–Condon simulation results for the transition state of the OH + H_2O reaction. *J. Phys. Chem. A* **125**, 2154–2162 (2021).
24. Y. Sugiura, T. Takayanagi, Franck–Condon simulations of transition-state spectra for the OH + H_2O and OD + D_2O reactions. *Phys. Chem. Chem. Phys.* **22**, 20685–20692 (2020).
25. H. Song, Y. Zhu, M. Pan, M. Yang, Dissociative photodetachment of $H_3O_2^-$: A full-dimensional quantum dynamics study. *Phys. Chem. Chem. Phys.* **23**, 22298–22304 (2021).
26. M. Masamura, Structures, energetics, and spectra of $OH^-(H_2O)_n$ and $SH^-(H_2O)_n$ clusters, n=1–5:*Ab initio* study. *J. Chem. Phys.* **117**, 5257–5263 (2002).
27. R.-J. Lin, Q. C. Nguyen, Y.-S. Ong, K. Takahashi, J.-L. Kuo, Temperature dependent structural variations of $OH^-(H_2O)_{n,\ n\ =\ 4\text{–}7}$: Effects on vibrational and photoelectron spectra. *Phys. Chem. Chem. Phys.* **17**, 19162–19172 (2015).
28. Q. Yuan, W. Cao, X.-B. Wang, Cryogenic and temperature-dependent photoelectron spectroscopy of metal complexes. *Int. Rev. Phys. Chem.* **39**, 83–108 (2020).
29. C. Møller, M. S. Plesset, Note on an approximation treatment for many-electron systems. *Phys. Rev.* **46**, 618–622 (1934).
30. G. D. Purvis III, R. J. Bartlett, A full coupled-cluster singles and doubles model: The inclusion of disconnected triples. *J. Chem. Phys.* **76**, 1910–1918 (1982).
31. K. Raghavachari, G. W. Trucks, J. A. Pople, M. Head-Gordon, A fifth-order perturbation comparison of electron correlation theories. *Chem. Phys. Lett.* **157**, 479–483 (1989).
32. T. H. Dunning Jr., Gaussian basis sets for use in correlated molecular calculations. I. The atoms boron through neon and hydrogen. *J. Chem. Phys.* **90**, 1007–1023 (1989).
33. G. Aravind, A. K. Gupta, M. Krishnamurthy, E. Krishnakumar, Photodetachment studies with the linear time of flight photoelectron spectrometer. *J. Phys. Conf. Ser.* **80**, 012026 (2007).
34. P. A. Schulz, R. D. Mead, P. L. Jones, W. C. Lineberger, OH^- and OD^- threshold photodetachment. *J. Chem. Phys.* **77**, 1153–1165 (1982).
35. J. R. Smith, J. B. Kim, W. C. Lineberger, High-resolution threshold photodetachment spectroscopy of OH^-. *Phys. Rev. A* **55**, 2036–2043 (1997).
36. M. DeWitt, M. C. Babin, D. M. Neumark, High-resolution photoelectron spectroscopy of vibrationally excited OH^-. *J. Phys. Chem. A* **125**, 7260–7265 (2021).
37. M. Meot-Ner, C. V. Speller, Filling of solvent shells about ions. 1. Thermochemical criteria and the effects of isomeric clusters. *J. Phys. Chem.* **90**, 6616–6624 (1986).
38. S. S. Xantheas, Theoretical study of hydroxide ion-water clusters. *J. Am. Chem. Soc.* **117**, 10373–10380 (1995).
39. H. Zhang, W. Cao, Q. Yuan, X. Zhou, M. Valiev, S. R. Kass, X.-B. Wang, Cryogenic "iodide-tagging" photoelectron spectroscopy: A sensitive probe for specific binding sites of amino acids. *J. Phys. Chem. Lett.* **11**, 4346–4352 (2020).
40. D. Hanstorp, M. Gustafsson, Determination of the electron affinity of iodine. *J. Phys. B At. Mol. Opt. Phys.* **25**, 1773 (1992).

41. X.-B. Wang, L.-S. Wang, Photodetachment of free hexahalogenometallate doubly charged anions in the gas phase: $[ML_6]^{2-}$, (M=Re, Os, Ir, Pt; L=Cl and Br). *J. Chem. Phys.* **111**, 4497–4509 (1999).
42. E. Miliordos, E. Aprà, S. S. Xantheas, Optimal geometries and harmonic vibrational frequencies of the global minima of water clusters $(H_2O)_n$, n = 2–6, and several hexamer local minima at the CCSD(T) level of theory. *J. Chem. Phys.* **139**, 114302 (2013).
43. E. Miliordos, S. S. Xantheas, An accurate and efficient computational protocol for obtaining the complete basis set limits of the binding energies of water clusters at the MP2 and CCSD(T) levels of theory: Application to $(H_2O)_m$, m = 2–6, 8, 11, 16, and 17. *J. Chem. Phys.* **142**, 234303 (2015).
44. M. Valiev, E. J. Bylaska, N. Govind, K. Kowalski, T. P. Straatsma, H. J. Van Dam, D. Wang, J. Nieplocha, E. Apra, T. L. Windus, NWChem: A comprehensive and scalable open-source solution for large scale molecular simulations. *Comput. Phys. Commun.* **181**, 1477–1489 (2010).
45. S. Hirata, Tensor contraction engine: Abstraction and automated parallel implementation of configuration-interaction, coupled-cluster, and many-body perturbation theories. *J. Phys. Chem. A* **107**, 9887–9897 (2003).
46. S. Hirata, Higher-order equation-of-motion coupled-cluster methods. *J. Chem. Phys.* **121**, 51–59 (2004).
47. S. Hirata, Symbolic algebra in quantum chemistry. *Theor. Chem. Acc.* **116**, 2–17 (2006).
48. S. Hirata, P.-D. Fan, A. A. Auer, M. Nooijen, P. Piecuch, Combined coupled-cluster and many-body perturbation theories. *J. Chem. Phys.* **121**, 12197–12207 (2004).
49. K. Kowalski, S. Hirata, M. Włoch, P. Piecuch, T. L. Windus, Active-space coupled-cluster study of electronic states of Be_3. *J. Chem. Phys.* **123**, 074319 (2005).

Acknowledgments
Funding: This work was supported by the U.S. Department of Energy (DOE), Office of Science, Office of Basic Energy Sciences, Division of Chemical Sciences, Geosciences, and Biosciences, Condensed Phase and Interfacial Molecular Science Program, FWP 16248 (X.-B.W.) and Molecular Theory and Modeling, FWP 16249 (S.S.X.) and performed using EMSL, a national scientific user facility sponsored by DOE's Office of Biological and Environmental Research and located at Pacific Northwest National Laboratory, which is operated by Battelle Memorial Institute for the DOE. Part of the calculations was carried out on EMSL's "Cascade" Supercomputer. This research also used resources of the National Energy Research Scientific Computing Center, which is supported by the Office of Science of the U.S. Department of Energy under contract no. DE-AC02-05CH11231. **Author contributions:** X.-B.W. and S.S.X. designed the research; W.C., H.W., S.S.X., and X.-B.W. conducted the research; W.C., S.S.X., and X.-B.W. analyzed the data; and W.C., S.S.X., and X.-B.W. wrote the paper. All authors contributed to the discussions. **Competing interests:** The authors declare that they have no competing interests. **Data and materials availability:** All data needed to evaluate the conclusions in the paper are present in the paper and/or the Supplementary Materials.

Submitted 20 October 2022
Accepted 22 February 2023
Published 24 March 2023
10.1126/sciadv.adf4309